Computational Energy Science

Vol. 1, No. 2, p. 117-126, 2024

Original article

Exploring critical size and critical temperature: Insights into adsorption and diffusion in nano confinement slits

Xueling Zhang[1,2]*, Qiang Ye[1], Sijie Shao[1], Yingfang Zhou[2]*, Weiyao Zhu[3], Hubao A[4], Wenfeng Hu[1]

[1]*School of Energy and Power Engineering, Zhengzhou University of Light Industry, Henan 450002, P. R. China*

[2]*School of Engineering, University of Aberdeen, Aberdeen, Scotland, United Kingdom, AB24 3UE*

[3]*School of Civil and Resource Engineering, University of Science and Technology Beijing, Beijing 100083, P. R. China*

[4]*School of Water Resources and Hydropower, Wuhan University, Hubei 430072, P. R. China*

Keywords:
Nano-slit
adsorption and diffusion
molecular simulation
critical size
critical temperature

Cited as:
Zhang, X., Ye, Q., Shao, S., Zhou, Y., Zhu, W., A, H., Hu, W. Exploring critical size and critical temperature: Insights into adsorption and diffusion in nano confinement slits. Computational Energy Science, 2024, 1(2): 117-126.
https://doi.org/10.46690/compes.2024.02.05

Abstract:
Nanoscale confinement affects unconventional oil and gas development, materials science, chemistry, and energy storage. Size and temperature significantly affect adsorption and diffusion, but the critical size and temperature for nano-confinement effects are not yet clear. In this study, molecular dynamics simulations were employed to investigate the n-heptane adsorption and diffusion characteristics of hydroxylated quartz in nano-confinement, the analysis elucidated that both size and temperature effects have important influences on adsorption and diffusion, the critical size is 6 nm, and the critical temperature is 303 K for the nano-confinement effect. Beyond 6 nm, a free adsorption layer appears, with constant absolute adsorption capacity and density peak value, and increased diffusion with increasing size and temperature, the interaction energy remains relatively constant with varying slit sizes. Below 6 nm, nano-confinement forms a fully adsorbed layer, absolute adsorption capacity decreases with increasing size, the interaction energy increases monotonically with decreasing slit sizes, the diffusion coefficient in the Z-direction is low to zero; The density peak value of the first adsorption layer increases and the diffusion coefficient decreases with decreasing size below 303 K; Below 6 nm and above 303K, the two values show little correlation with size and exhibit somewhat random fluctuations, suggesting that temperatures exceeding 303 K weaken the nanoconfinement effect. This paper provides certain theoretical guidance for the development of fluids in nanopores such as shale oil.

1. Introduction

With the reduction of conventional oil and gas reserves, the development of unconventional oil and gas such as shale oil has now become an important part of the world's energy replacement (Hughes, 2013; Liang et al., 2022). Scholars have conducted extensive research for the slit architecture of shale through microscale experimental techniques, including high-pressure pumping (Chen et al., 2017), atomic force microscopy (AFM) (Perez and Devegowda, 2019), scanning electron microscopy (SEM) (Vishal et al., 2019), and gas adsorption (Xu, 2020). Their findings reveal that shale reservoirs have complex microstructures, mainly consisting of nanoscale slits with very low porosities (10%) and permeabilities (1-10 nD) (Lee and Kim, 2016; Liu et al., 2017).

In shale reservoirs, especially within nanoslits, there is a strong interaction between the fluid and the slit walls. This causes a significant nano-confinement effect on the fluid molecules, making their behavior very different from that in larger-scale environments (Yu et al., 2020). This nano-confinement effect is seen in the way the fluid is adsorbed onto the slit walls, leading to noticeable changes in important properties, such as stronger adsorption and weaker diffusion compared to those in the bulk phase (Bicerano, 2012).

To explore the thermodynamic and kinetic attributes of shale oil under nano-constrained circumstances, researchers

Yandy Scientific Press

*Corresponding author.
E-mail address: zhangxueling268@163.com (X. Zhang); qiangye2023@163.com (Q. Ye); sijieshao@foxmail.com (S. Shao); yingfang.zhou@abdn.ac.uk (Y. Zhou); weiyaook@sina.com (W. Zhu); a_hubao@whu.edu.cn (H. A).

Received April 11, 2024; revised May 17, 2024; accepted June 17, 2024; available online June 20, 2024.

have devised an array of experimental and simulation techniques, encompassing adsorption-desorption (Rogala et al., 2017), differential scanning calorimetry (Kodali, 2005), and nanochannel methodologies (Mino and Kazoe, 2023). Simulation methodologies encompass density-functional theory (Zheng et al., 2021), molecular dynamics (Sonibare et al., 2021), lattice Boltzmann modeling (Rong et al., 2010), equation of state analysis (Yang et al., 2019), and machine learning techniques (Li et al., 2021). Nevertheless, conventional physical experimental approaches are constrained to evaluating the adsorption kinetics and capacity of individual components, thus failing to systematically elucidate the microscopic characteristics within nanoslits, let alone guaranteeing result accuracy (Akbarabadi et al., 2017; Chen et al., 2017). Molecular simulation (MD), recognized as an efficacious tool for characterizing the microscopic behavior of substances, offers a comprehensive assessment of intermolecular and wall-fluid interactions, thus finding extensive application in shale oil adsorption studies (Huang et al., 2021; Chang et al., 2022).

Researchers have extensively investigated temperature and slit size as crucial factors influencing the adsorption dynamics of shale oil. Xiong et al. (2016) explored the fugacity state of methane within quartz nanoslits, observing the formation of adsorption phases near the slit wall due to its strong attraction. At 300 K, a reduction in slit size resulted in increased adsorption, whereas elevated temperatures led to decreased adsorption. Zhang et al. (2017) replaced varying depths with different temperature pressures and observed methane adsorption in 2.5 nm carbon nanotube slits, noting a trend of initially increasing and then decreasing adsorption with rising temperature pressure. Huai et al. (2020) found that the average potential energy of methane molecules in nanoslits is lower than that of water molecules. Bekeshov et al. (2023) discovered that as the slit slit width increases, the adsorption amount of gas molecules also increases, and the number density distribution of adsorbed methane molecules transitions from monolayer to multilayer adsorption. Xu et al. (2023) examined the adsorption characteristics of liquid alkanes in organic nanoslits, observing that at a specific temperature pressure (383 K, 20 MPa), alkane adsorption was confined within 3.6 nm. Beyond this threshold, alkane behavior transitioned from solely adsorbed to a coexistence of adsorbed and free states, with the peak of each adsorbent layer increasing with slit size. Chen et al. (2019) discovered that methane adsorbed within montmorillonite nanoslits exhibited a critical slit size of 2 nm, with complete adsorption in slits < 2 nm. At a slit size of 1 nm, methane remained exclusively in the adsorbed state, while slits ≥ 2 nm featured a free zone. The thickness of the adsorbed zone is no longer affected by slit size and pressure. Cui et al. (2022) developed a molecular model of Gulong shale oil and found that changes in the content of polar components lead to more significant variations in the physical properties of shale oil compared to changes in hydrocarbon content. Sun et al. (2023) observed that light oil alkanes predominantly existed in the adsorbed state within slits narrower than 3 nm, while both adsorbed and free states coexisted in larger slits. Fang et al. (2024) examined the adsorption behavior of n-octane on the kerogen-illite heterogeneous, observing rapid decreases in the percentage of the first adsorption layer to total adsorption as slit size increased. This effect was pronounced at 353 K and 30 MPa, indicating a temperature-induced reduction. Fei et al. (2023) observed that elevated temperatures facilitated the desorption of oil molecules from adsorption sites, resulting in decreased adsorption and increased uptake by casein. Conversely, pressure and slit size exerted minimal influence on shale oil distribution. Wang (2016) discovered that widening the slit slits of graphite led to a gradual increase in the average density of the adsorbed fluid. However, this trend eventually stabilized, reaching a constant value.

In conclusion, the adsorption of shale oil in shale reservoirs is influenced by three primary factors: Pressure, temperature, and slit size. However, ongoing controversy among researchers regarding the analysis of temperature and slit size stems from the research paradigm, which often focuses on studying slit size at a constant temperature or temperature at fixed slit size conditions. This approach fails to systematically and comprehensively account for the nanoconfinement effect of shale oil across varying temperatures and size.

This study utilizes molecular dynamics simulation, using n-alkanes as a substitute for shale oil, to analyze the adsorption and diffusion behavior of shale oil in quartz nanoslits. It considers the effects of different temperatures (283 K to 363 K) and slit sizes (2 nm to 10 nm) on shale oil adsorption and diffusion, and identifies the critical size and critical temperature for the nano confinement effect on adsorption and diffusion. The results elaborate on the adsorption mechanism, providing theoretical insights for the future efficient development of shale oil resources.

2. Models and methods

2.1 Molecular models

Throughout the evolution of shale sedimentary rocks, typically saturated by aquifers prior to hydrocarbon generation, the quartz surface within the formation becomes fully hydroxylated, exhibiting pronounced hydrophilicity (Skelton et al., 2011). Consequently, this paper initially adopts the hydroxylated quartz model to construct slit-like shale slits. The monomer model of quartz is sourced from the Cambridge Structural Crystal Database (CSDS), with its monomer cell depicted in Fig. 1(a). Building upon this foundation, slicing and cell expansion procedures were conducted on the (100) face of the quartz monocrystalline cell model, followed by hydroxylation of the quartz surface, resulting in a quartz supercell structure measuring 2.948 nm $\times$ 2.703 nm in the x and y directions, respectively, as illustrated in Fig. 1(b).

Shale oil exhibits a highly intricate composition, comprising diverse compounds including n-alkanes, branched alkanes, aromatic hydrocarbons, and asphaltenes (Jorgensen et al., 1996). Following the construction of the n-heptane monomer model, structural optimization is necessary to derive the stable molecular model of heptane. Subsequently, a specific quantity of n-heptane molecules was chosen to construct the liquid box depicted in Fig. 2(a), with box dimensions in the x and y directions aligned with the parameters of the wall model shown in Fig. 1(b). Subsequently, the wall model and

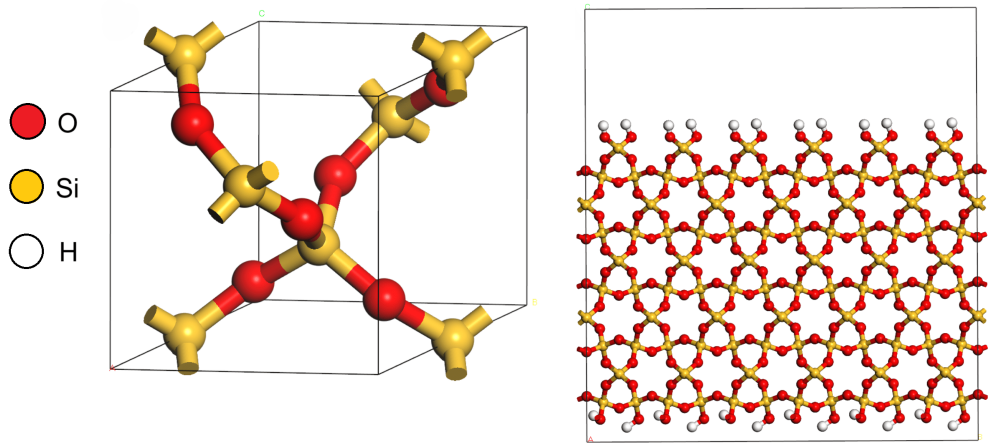

(a) (b)

Fig. 1. Quartz cell model: (a) single cell model; (b) supercell model.

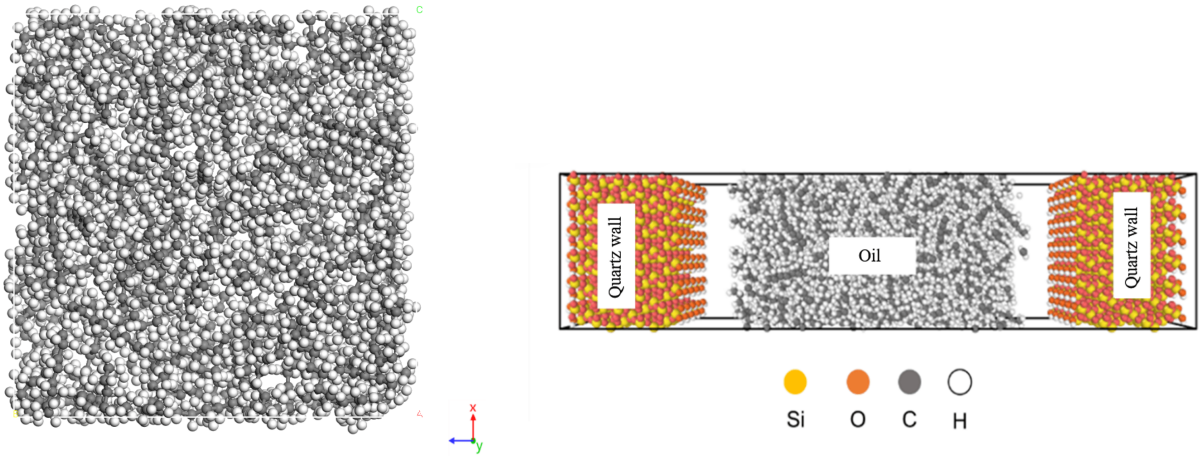

(a) (b)

Fig. 2. Initial adsorption configuration: (a) n-heptane box; (b)nano-slit box.

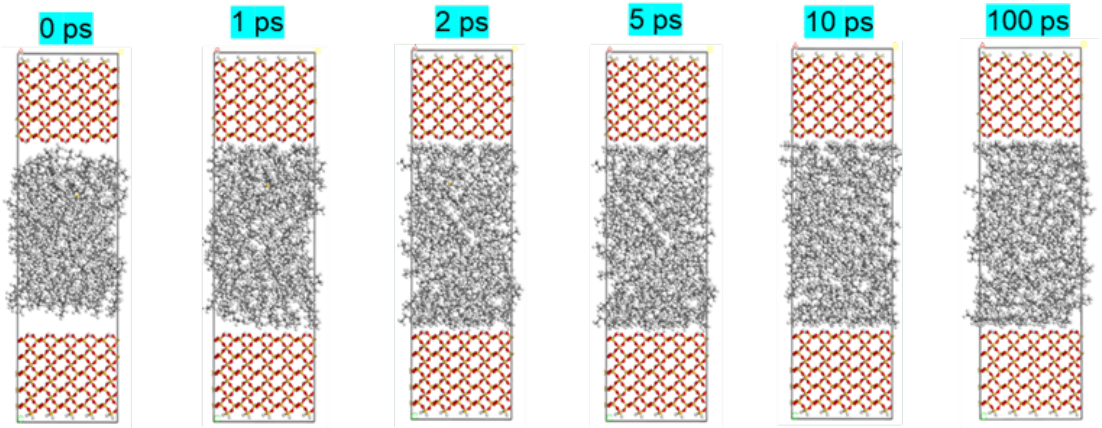

Fig. 3. Relaxation process of n-heptane adsorption system.

the liquid model were integrated to form the initial model of shale oil in quartz nanoslits, as illustrated in Fig. 2(b). The slit aperture values considered in this paper range from 2 to 10 nm.

2.2 Simulation methods

The entirety of the simulation process was executed using the large-scale atomic/molecular massively parallel simulator (LAMMPS), with the results subsequently visualized via OVITO. In this study, n-heptane was chosen as the subject of investigation. The OPLS force field was employed for n-heptane, while the CLAYFF force field was utilized for the quartz wall surface. The system incorporated periodic boundary conditions. The van der Waals potential was calculated via the Atom summation method, and the electrostatic potential was computed using the Ewald summation method, with a truncation radius of 12.5 Å. During the simulation, following the minimization of system energy, the upper and lower quartz wall surfaces were fixed. The NVT ensemble was then applied to the system for 2 ns. The system was subsequently subjected to a 2 ns interval. Post energy minimization, the upper and lower quartz wall surfaces remained fixed, and kinetic relaxation was achieved via the NVT ensemble for 2 ns, maintaining constant molecule count, volume, and temperature throughout the relaxation period. The timestep was set to 1 fs, and a Nose-Hoover thermostat was utilized for temperature regulation. The total simulation spanned 2,000,000 steps, with one frame output every 20,000 steps. Upon completion of the relaxation phase, the equilibrated atomic trajectories were collected for statistical analysis. The specific adsorption process is illustrated in Fig. 3.

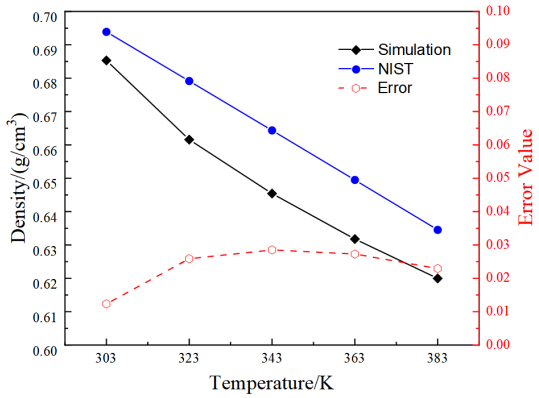

Fig. 4. Comparison of simulated and standard values of n-heptane density.

2.3 Force field validation

To verify the applicability of the OPLS force field to n-heptane fluid, this study constructs a fluid box containing 1000 n-heptane molecules with an initial density of 1 g/cm^3. The OPLS potential is applied to the fluid box. To prevent atomic overlap and consequent high energy, the smart algorithm is first employed to minimize system energy. Subsequently, NPT dynamics relaxation is performed for 2 ns, followed by NVT dynamics relaxation for an additional 2 ns. The density of n-heptane is then statistically analyzed and compared with the NIST density value at the same temperature and pressure. During NVT kinetic relaxation, the system pressure is maintained at 20.7 MPa. The final density of n-heptane is statistically analyzed and compared with the NIST density value at identical temperature and pressure conditions. As shown in Fig. 4, the discrepancy between the simulated value and the NIST standard is within 5%, thus confirming the validity of the OPLS force field.

3. Results and discussion

3.1 Spatial distribution characteristics of n-heptane in quartz nanoslits

The density of n-heptane molecules within the system was calculated by partitioning the simulated area. Fig. 5 illustrates the density distribution curve of n-heptane in an 8 nm quartz nanoslits at a temperature of 353 K. The figure reveals that n-heptane exhibits inhomogeneous distribution characteristics within the nanoslit, attributed to the interaction between the quartz wall and n-heptane molecules. This results in the formation of an adsorption zone with oscillating density and a free zone with uniform density. This oscillatory layering near the wall represents the multilayer adsorption of molecules, while the smooth density distribution in the center signifies the free state of the molecules, as has been demonstrated by several studies (Sui et al., 2020; Zhang et al., 2022). Multiple adsorption layers are formed within the adsorption zone, with the peak density of the adsorption layers increasing as they approach the slit wall. Notably, the peak density of the first adsorption layer near the slit wall is 1.24 g/cm^3, approximately 1.89 times the density of the free state, thus forming a ”solid-like layer.” In the free zone distant from the wall, the density of n-heptane approaches the bulk value of 0.65694 g/cm^3 (NIST standard value), thereby confirming the accuracy of the shale oil adsorption model.

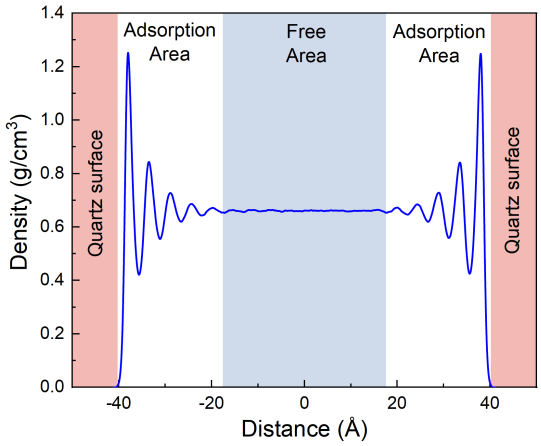

Fig. 5. Density distribution curve of n-heptane on quartz wall.

3.2 Characterization of n-heptane adsorption at constant temperature across varied slit sizes

Fig. 6 illustrates the density distribution of n-heptane within six quartz nanoslits, each with varying slit size, at

a temperature of 323 K. The figure reveals that n-heptane adsorption within quartz nanoslits is confined by a critical size of 6 nm. When the slit size is less than 6 nm, n-heptane molecules are entirely in an adsorbed state throughout the slit space. This complete adsorption is attributed to the cumulative effect of forces from both slit walls, and the number of adsorption layers increases with increasing slit size. When the slit size exceeds 6 nm, the number of adsorption layers remains constant. A symmetric arrangement of five adsorption layers forms near the quartz wall surface, while the heptane molecules at the slit center remain in a free state, largely unaffected by alkane-wall interactions, with a density approaching that of the bulk phase.

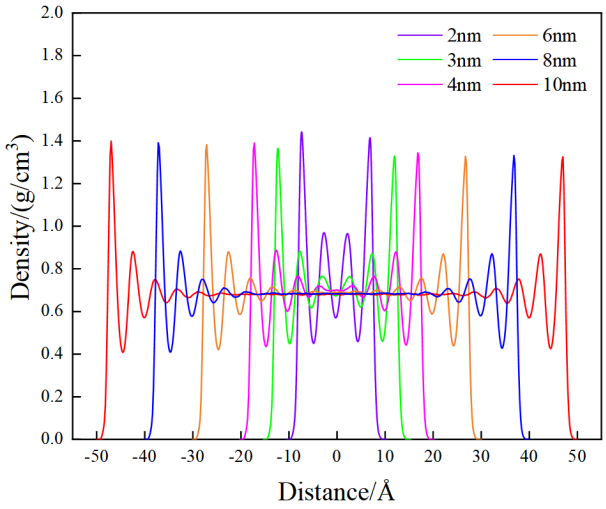

Fig. 6. Density distribution of n-heptane at different slit sizes.

3.3 Characterization of n-heptane adsorption across varied temperatures and slit sizes

Fig. 7 presents the density distribution curves of n-heptane at five distinct temperatures, ranging from 283 to 363 K, within six quartz slits of varying slit sizes, from 2 to 10 nm. The figure illustrates that within the six quartz nanoslits of varying slit sizes, an increase in temperature exerts an inhibitory effect on n-heptane adsorption. When the slit size is less than 6 nm, the density distribution does not reach a steady state across the slit but instead exhibits multiple oscillating peaks and troughs. We interpret these as multilayer adsorption, a phenomenon observed in other studies as well (Zhang et al., 2019; Sui et al., 2020), and the n-heptane is entirely in the adsorbed state. For a given slit size, the peak densities of adsorption layers at temperatures below 303 K are significantly higher compared to other temperatures. As the temperature increases from 323 to 363 K, the peak density of the adsorption layer decreases progressively. However, when the slit size is extremely small (less than 2 nm), the temperature-induced trend in peak density becomes less pronounced, as depicted in Fig. 7. When the slit size exceeds or equals 6 nm, n-heptane transitions to a free state away from the wall. The density difference due to low temperatures (below 303 K) diminishes, and both the peak density of the adsorbed layer and the density of the free phase gradually decrease as the temperature ranges from 283 to 363 K. Furthermore, the temperature-induced density difference lessens as the slit size increases.

To investigate the variation in adsorption characteristics of n-heptane with slit size at different temperatures, Fig. 8 analyzes the adsorption quantity of n-heptane at various slit sizes and temperatures, as well as the peak value of the first adsorbed layer. Fig. 8(a) reveals that the absolute adsorption capacity Γ_{ab} increases progressively with slit size and stabilizes upon reaching 6 nm. These quantities are calculated using Eq. (1):

$$\Gamma_{ab} = V_{ad}\rho_{ad} \tag{1}$$

where V_{ad} is the volume of the adsorption region, ρ_{ad} is the average density of the adsorption region.

Furthermore, the adsorption quantity decreases with rising temperatures from 283 to 363 K, with a diminishing rate of decrease, indicating that the increase in adsorption quantity is more pronounced at lower temperatures. Fig. 8(b) shows the relationship between the peak value of the first adsorption layer and the temperature and slit size, it decreases with increasing temperature, and it is demarcated by a slit size of 6 nm. When the slit size exceeds 6 nm, the peak value of the first adsorption layer remains unchanged with slit size. Conversely, when the slit size is less than 6 nm, influenced by the slit size effect, the peak value of the first adsorption layer exhibits undulations with decreasing slit size at temperatures above 323 K, showing random variations at different temperatures. When the temperature is below 303 K, the peak value of the first adsorption layer increases with decreasing slit size, and the nano-confinement effect is obvious. As the temperature rises, the peak density of the first adsorption layer decreases, which shows that the size constraint effects are weak.

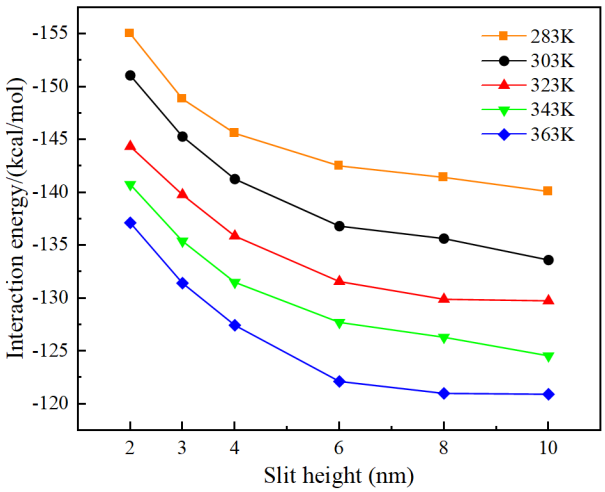

Fig. 9. Curves of interaction energy between n-heptane molecules and walls as a function of slit size and temperature.

To elucidate the underlying reasons for the observed phenomenon, Fig. 9 analyzes the variation in interaction energy between n-heptane and the quartz wall surface across different slit sizes under five distinct temperature conditions. The results shows that the interaction energy between n-heptane and the

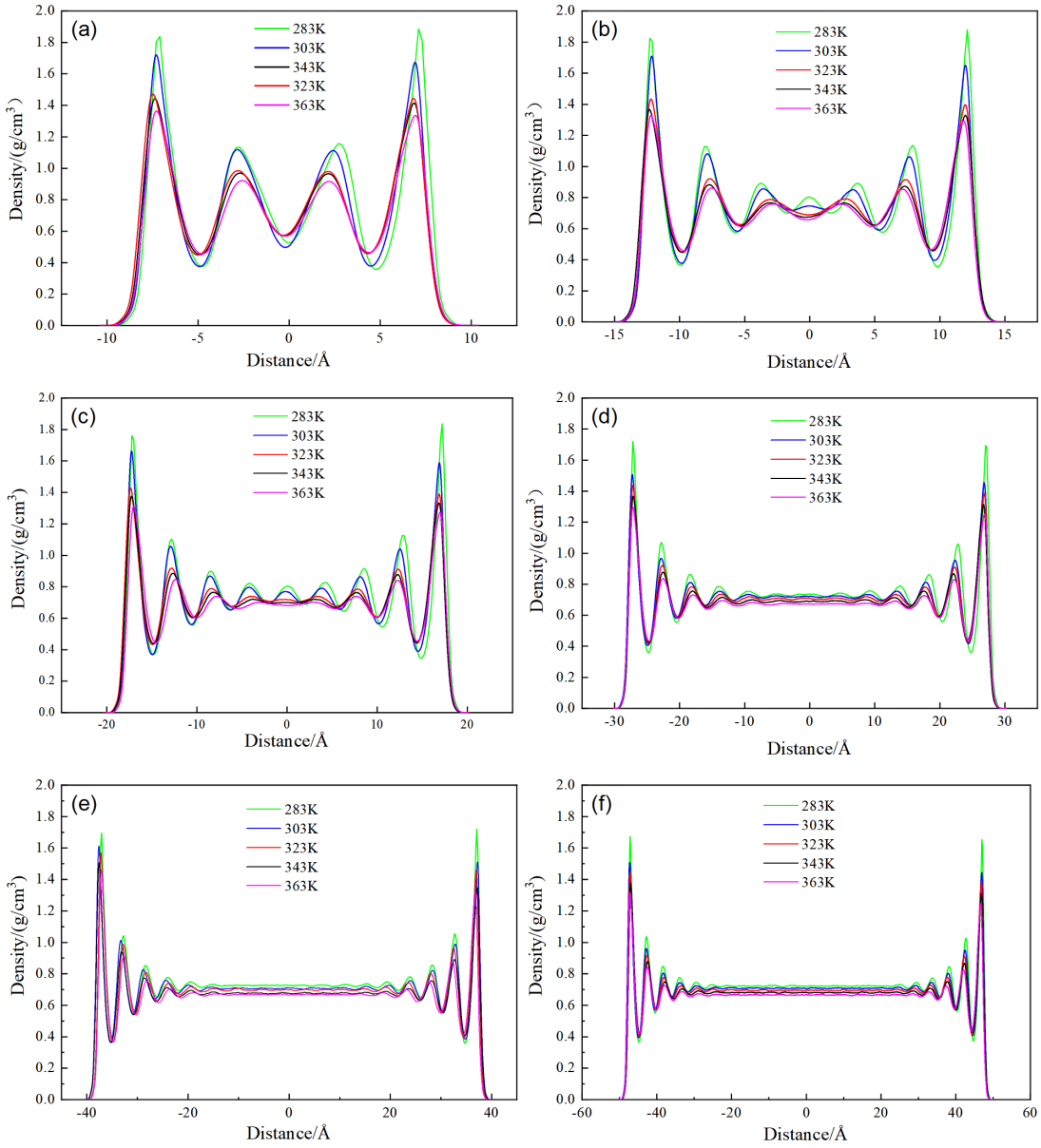

Fig. 7. Density distribution curves of n-heptane in (a) 2 nm, (b) 3 nm, (c) 4 nm, (d) 6 nm, (e) 8 nm and (f) 10 nm quartz slits at different temperatures.

quartz wall surface decreases with rising temperature. For slit sizes greater than 6 nm, the interaction energy remains relatively constant with varying slit sizes, and it increases monotonically with decreasing slit sizes due to the superposition effect from both sides of the wall when slit size is smaller than 6 nm. At low temperatures (below 303 K), the interaction energy between n-heptane and the wall surface is significantly enhanced, dominating the adsorption process. This results in an increase in the peak size of the first adsorption layer with decreasing slit size. Conversely, at high temperatures (above 323 K), the adsorption energy is low and thermal motion is accelerated. Together, these factors result in the first adsorption layer being minimally affected by the slit size, showing little change with varying scale, as illustrated in Fig. 8(b).

3.4 Diffusion characterization of n-heptane across varied temperatures and slit sizes

Throughout the simulation process, heptane molecules exhibit erratic movement within the slit, primarily driven by intermolecular interactions, rendering their diffusion behavior highly susceptible to variations in temperature and slit size. In investigations concerning shale oil adsorption properties, the diffusion capacity of oil molecules is evaluated through the diffusion coefficient. The diffusion coefficient D is calculated using the following Eq. (2):

$$D = \lim_{t\to\infty} \frac{1}{4N_m t} \left\langle \sum_{j=1}^{N_m} [r_j(t) - r_j(0)]^2 \right\rangle \tag{2}$$

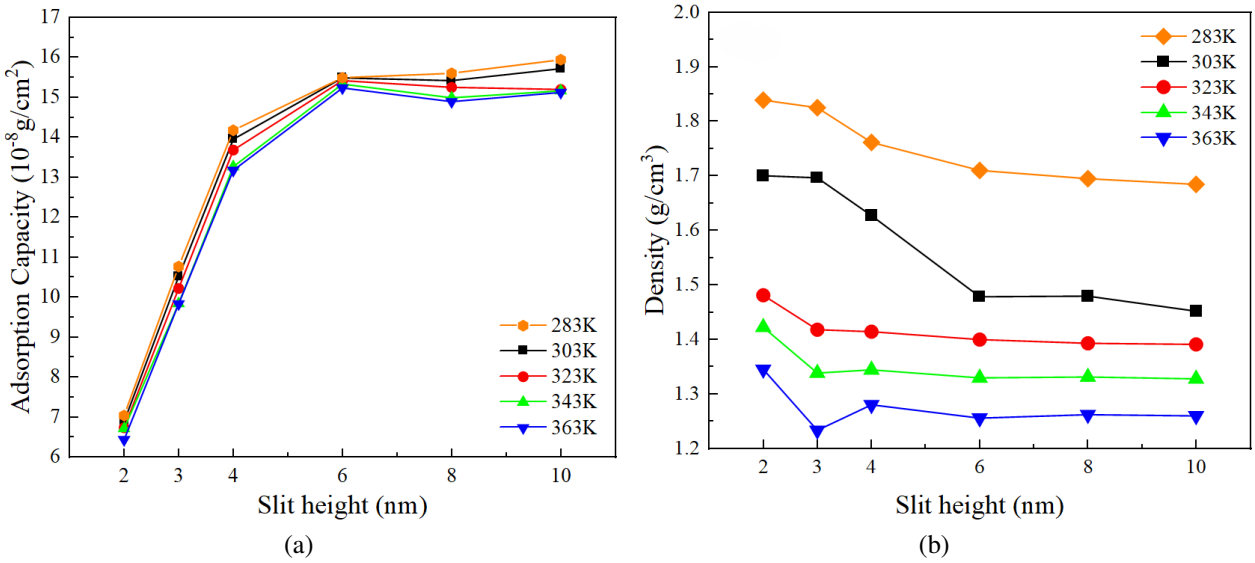

Fig. 8. Adsorption of n-heptane at different slitsizes and different temperatures for (a) absolute adsorption capacity and (b) peak density of the first adsorption layer.

where N_m is the number of particles, $r_j(t)$ is the position of particle j at time t, $\sum_{j=1}^{N_m}[r_j(t)-r_j(0)]$ is the mean square displacement (MSD).

Fig. 10 presents the total diffusion coefficient of n-heptane across various slit sizes at different temperatures. Observably, at constant slit size, the total diffusion coefficient rises with temperature as the temperature escalates from 283 to 363 K. This phenomenon stems from the heightened thermal agitation of n-heptane molecules at elevated temperatures, consequently augmenting their diffusive behavior. The diffusion coefficient escalates with enlarging slit size for sizes exceeding 6 nm. Conversely, for sizes below 6 nm, the diffusion coefficient exhibits a negligible trend with slit size at elevated temperatures (323K-363K), and precipitously declines with diminishing slit size at lower temperatures (below 303K), underscoring the pronounced influence of size at low temperatures.

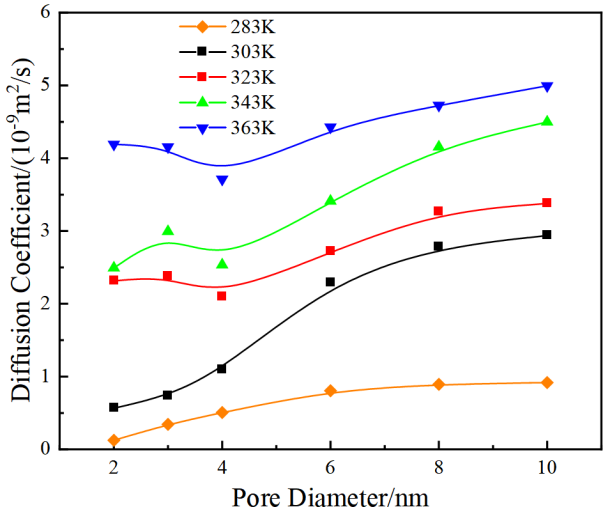

Fig. 10. The variation curve of total diffusion coefficient of n-heptane with slit size at different temperatures.

Figs. 11(a) and 11(b) show the diffusion coefficients of n-heptane in the Z direction and X-Y plane at various temperatures as a function of slit size. Analysis of Fig. 11(a) reveals that in the Z direction, for slit sizes smaller than 6 nm, the diffusion coefficient remains very low, stabilizing in the range of 0 to 2 $\times$ 10^{-10} m^2/s, with a slow increase as the slit size increases, and temperature has no significant effect. However, for slit sizes greater than or equal to 6 nm, the diffusion coefficient in the Z direction rises rapidly to a higher value and then increases more gradually, with a notable increase as temperature rises. This indicates that the diffusion coefficient in the Z direction is strongly influenced by the slit size, with 6 nm serving as a critical threshold, while the effect of temperature is relatively weak.

For Fig. 11(b), the diffusion coefficient in the X-Y plane generally increases significantly with rising temperature, but there is no clear pattern of variation with slit size. However, at lower temperatures below 303 K, the diffusion coefficient in the X-Y plane decreases progressively as slit size decreases, especially for sizes below 6 nm, where it drops to a much lower range. Therefore, for diffusion in the X-Y plane, it can be concluded that the low temperature of 303 K induces different trends in the diffusion coefficient, with a particularly strong impact on diffusion for slit sizes smaller than 6 nm.

Analysis of the total diffusion coefficient involved a combination of the diffusion coefficients in both the Z direction and X-Y direction. It was observed that the total diffusion coefficient exhibited an overall increase with rising temperature. However, a pronounced nano confinement effect was evident for the diffusion the Z direction, there is weak diffusion occurred in the Z direction for slit sizes less than 6 nm. The diffusion coefficient in the X-Y direction decreased with decreasing slit size at low temperatures (below 303 K), the especially for sizes below 6 nm, where it drops to a much lower range. At elevated temperatures, the nano confinement

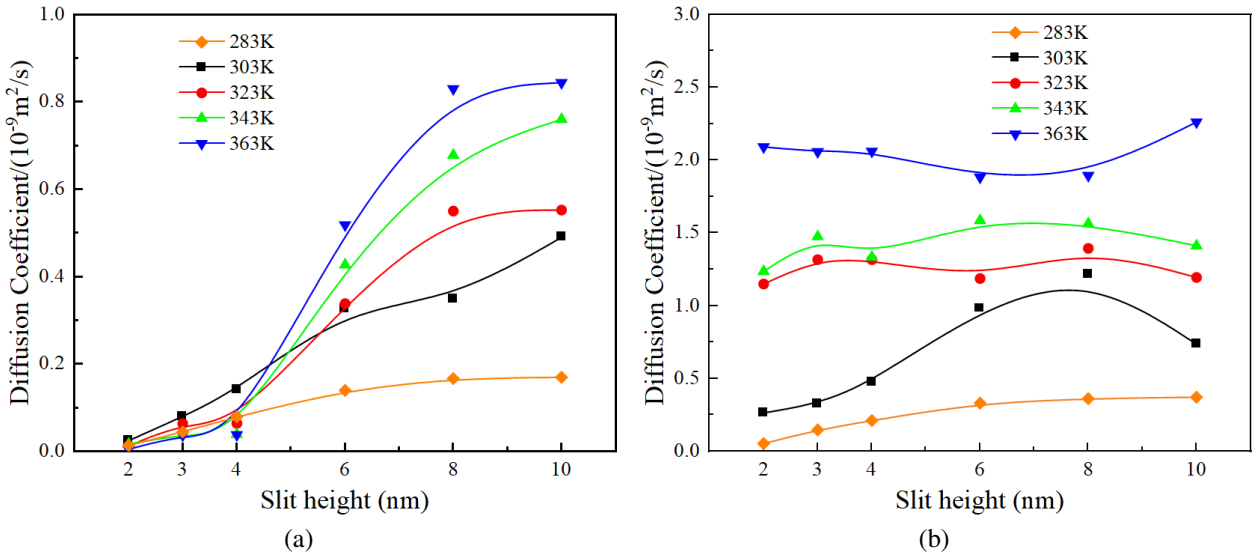

Fig. 11. Diffusion coefficients of n-heptane with slit height along (a) Z and (b) X-Y directions in slit at different temperatures.

effect became insignificant due to thermal motion in the X-Y direction.

4. Conclusions

This study investigates the adsorption and diffusion characteristics of n-heptane molecules in quartz nanoslits using molecular dynamics simulations. The research focuses on identifying the critical slit size and critical temperature for adsorption and diffusion behavior under nano-confinement. Through detailed analysis of the density distribution, absolute adsorption capacity, peak density of the first adsorption layer, interaction energy, and diffusion coefficients, the study has led to the following key findings:

When the slit size exceeds 6 nm, both an adsorbed layer and a free layer appear. The absolute adsorption capacity and the peak density of the first adsorption layer are stable with the increase of slit size, and only decrease with the increase of temperature. When it is less than 6 nm, it is mainly the adsorption area, the absolute adsorption capacity increases significantly with the decrease in size. When the temperature is lower than 303 K, the density of the first adsorption layer increases as the size decreases. This trend is obvious because the adsorption activation energy increases with the decrease of temperature and size. When the temperature is higher than 303 K, the peak value of the first adsorption layer basically does not change. This is because the thermal motion of molecules intensifies as the temperature increases, which weakens this nano confinement effect.

For slit sizes larger than 6 nm, the total diffusion coefficient and the X-Y and Z-direction diffusion coefficients generally increase with increasing slit size and temperature. For small slit sizes (less than 6 nm), the Z-direction diffusion coefficient is generally lower to zero. At low temperatures (303 K), the total and X-Y diffusion coefficient decreases with decreasing slit size due to the enhancement of nano-confinement effect at low temperature. Above 303 K, the total diffusion coefficient and the X-Y direction diffusion coefficient remain stable with the size due to the thermal motion at high temperatures weakens the size constraints.

This paper explores the critical size and critical temperature for adsorption and diffusion within nano-confinement, providing valuable insights for understanding the occurrence mechanism and flow development of shale oil. Future research can further explore the critical temperature and critical size for the flow of actual shale oil within the kerogen system.

Author information

The email addresses of the remaining authors of this paper are as follows:

hwf@zzuli.edu.cn (W. Hu).

Acknowledgements

We would like to express appreciation to the following financial support: National Natural Science Foundation of China (No.51604245), and Henan Province Key R & D and Promotion Special (Science and Technology Tackling) Program (No.232102320201), 2023 Henan Province Undergraduate College Young Backbone Teacher Training Plan Project (No.2023GGJS089)

Conflict of interest

The authors declare no competing interest.

References

Akbarabadi, M., Saraji, S., Piri, M., et al. Nano-scale experimental investigation of in-situ wettability and spontaneous imbibition in ultra-tight reservoir rocks. Advances

in Water Resources, 2017, 107: 160-179.

Bekeshov, D., Ashimov, S., Wang, Y., et al. Understanding gas-enhanced methane recovery in graphene nanoslits via molecular simulations. Capillarity, 2023, 6(1): 1-12.

Bicerano, J. Thermoset particles with enhanced crosslinking, production, and their use in oil and natural gas drilling applications. US20110245473A1(P), 2012.

Chang, C., Zhang, J., Hu, H., et al. Molecular simulation of adsorption in deep marine shale gas reservoirs. Energies, 2022, 15(3): 944.

Chen, C., Hu, W., Sun, J., et al. CH_4 adsorption and diffusion in shale pores from molecular simulation and a model for CH_4 adsorption in shale matrix. International Journal of Heat and Mass Transfer, 2019, 141: 367-378.

Chen, G., Lu, S., Zhang, J., et al. Keys to linking GCMC simulations and shale gas adsorption experiments. Fuel, 2017, 199: 14-21.

Cui, F., Jin, X., Liu, H., et al. Molecular modeling on Gulong shale oil and wettability of reservoir matrix. Capillarity, 2022, 5(4): 65-74.

Chen, L., Jiang, Z., Liu, K., et al. Slit structure characterization for organic-rich Lower Silurian shale in the Upper Yangtze Platform, South China: A possible mechanism for slit development. Journal of Natural Gas Science and Engineering, 2017, 46: 1-15.

Fang, Y., Li, Z., Yang, E., et al. Molecular Dynamics Simulation Study on the Occurrence of Shale Oil in Hybrid Nanopores. Molecules, 2024, 29(2): 312.

Fei, J., Wang, M., Li, J., et al. Molecular dynamics simulation of adsorption and absorption behavior of shale oil in realistic kerogen slits. Energy & Fuels, 2023, 37(5): 3654-3671.

Huai, J., Xie, Z., Li, Z., et al. Displacement behavior of methane in organic nanochannels in aqueous environment. Capillarity, 2020, 3(4): 56-61.

Huang, L., Zhou, W., Xu, H., et al. Dynamic fluid states in organic-inorganic nanocomposite: Implications for shale gas recovery and CO_2 sequestration. Chemical Engineering Journal, 2021, 411: 128423.

Hughes, J. D. A reality check on the shale revolution. Nature, 2013, 494(7437): 307-308.

Jorgensen, W. L., Maxwell, D. S., Tirado-Rives, J. Development and testing of the OPLS all-atom force field on conformational energetics and properties of organic liquids. Journal of the american chemical society, 1996, 118(45): 11225-11236.

Kodali, D. R. Oxidative stability measurement of high-stability oils by pressure differential scanning calorimeter (PDSC). Journal of agricultural and food chemistry, 2005, 53(20): 7649-7653.

Lee, K. S., Kim., T. H. Integrative understanding of shale gas reservoirs. Heidelberg: Springer, 2016.

Li, Q., Wittreich, G., Wang, Y., et al. Accurate thermochemistry of complex lignin structures via density functional theory, group additivity, and machine learning. ACS Sustainable Chemistry & Engineering, 2021, 9(8): 3043-3049.

Liang, S., Wang, J. M., Liu, Y. K., et al. Oil occurrence states in shale mixed inorganic matter nanopores. Frontiers in Earth Science, 2022, 9: 833302.

Liu, K., Ostadhassan, M., Zhou, J., et al. Nanoscale pore structure characterization of the Bakken shale in the USA. Fuel, 2017, 209: 567-578.

Mino, K., Kazoe, Y. Hydrophobic and oleophobic nanopillars reduce viscous drag in slit nanofluidic channels. Applied physics letters, 2023, 123(7).

Perez, F., Devegowda, D. Spatial distribution of reservoir fluids in mature kerogen using molecular simulations. Fuel, 2019, 235: 448-459.

Rogala, Z., Kolasiński, P., Gnutek, Z. Modelling and experimental analyzes on air-fluidised silica gel-water adsorption and desorption. Applied Thermal Engineering, 2017, 127: 950-962.

Rong, F., Guo, Z., Chai, Z., et al. A lattice Boltzmann model for axisymmetric thermal flows through porous media. International Journal of Heat and Mass Transfer, 2010, 53(23-24): 5519-5527.

Skelton, A. A., Fenter, P., Kubicki, J. D., et al. Simulations of the quartz (1011)/water interface: a comparison of classical force fields, ab initio molecular dynamics, and X-ray reflectivity experiments. The Journal of Physical Chemistry C, 2011, 115(5): 2076-2088.

Sonibare, K., Rucker, G., Zhang, L. Molecular dynamics simulation on vegetable oil modified model asphalt. Construction and Building Materials, 2021, 270: 121687.

Sui, H., Zhang, F., Wang, Z., et al. Molecular simulations of oil adsorption and transport behavior in inorganic shale. Journal of Molecular Liquids, 2020, 305: 112745.

Sun, L., Jia, N., Feng, C., et al. Exploration of Oil/Water/-Gas Occurrence State in Shale Reservoir by Molecular Dynamics Simulation. Energies, 2023, 16(21): 7253.

Vishal, V., Chandra, D., Bahadur, J., et al. Interpreting pore dimensions in gas shales using a combination of SEM imaging, small-angle neutron scattering, and low-pressure gas adsorption. Energy & Fuels, 2019, 33(6): 4835-4848.

Wang, S. Research on microscale flow mechanism of shale oil. Qingdao: China University of Petroleum (East China), 2016.

Xiong, J., Liu, K., Liu, X., et al. Molecular simulation of methane adsorption in slit-like quartz pores. RSC advances, 2016, 6(112): 110808-110819.

Xu, H. Probing nanopore structure and confined fluid behavior in shale matrix: A review on small-angle neutron scattering studies. International Journal of Coal Geology, 2020, 217: 103325.

Xu, J., Wang, R., Zan, L. Shale oil occurrence and slit medium coupling based on a molecular dynamics simulation. Journal of Petroleum Science and Engineering, 2023, 220: 111151.

Yang, Z. L., Yu, H. Y., Chen, Z. W., et al. A compositional model for CO_2 flooding including CO_2 equilibria between water and oil using the Peng–Robinson equation of state with the Wong–Sandler mixing rule. Petroleum Science, 2019, 16(4): 874-889.

Yu, H., Xu, H., Fan, J., et al. Transport of shale gas in

microporous/nanoporous media: molecular to pore-scale simulations. Energy & Fuels, 2020, 35(2): 911-943.

Zhang, D., Tang, H., Zhang, X., et al. Molecular simulation of methane adsorption in nanoscale rough slits. Journal of Natural Gas Science and Engineering, 2022, 102: 104608.

Zhang, T., He, Y., Yang, Y., et al. Molecular simulation of shale gas adsorption in organic-matter nanopore. Journal of Natural Gas Geoscience, 2017, 2(5-6): 323-332.

Zhang, W., Feng, Q., Wang, S., et al. Oil diffusion in shale nanopores: Insight of molecular dynamics simulation. Journal of Molecular Liquids, 2019, 290: 111183.

Zheng, H., Liu, C., Cai, S., et al. Investigation of the palm oil-solubility in naphthenic insulating oil using density functional theory and COSMO-RS. Computational and Theoretical Chemistry, 2021, 1198: 113184.